Digitally Controlled Energy Harvesting Power Management System

Andrew Jordan Dickson, *Student Member, IEEE*, Sarah Burton, Michael Shepertycky, Yan-Fei Liu, *Fellow, IEEE*, and Qingguo Li

***Abstract*— Intermittent energy harvesting devices often have difficulties in harvesting the peak energy generated due to battery power limitations, which increase the size and cost of the device. This paper discusses a power electronics module (PEM) that is used to extract power from a human energy harvesting device according to the user's desired difficulty level while maximizing energy transfer into a battery. The PEM can temporarily store the peak power produced by the generator, allowing a reduction in the battery size required to regulate the average power produced by the harvester. A two-stage prototype (a digitally controlled average current mode boost converter and an average current mode buck converter) has been designed, and the experimental waveforms were captured to validate the control theories used in the PEM. The peak efficiencies of the boost and buck are measured to be 93% and 93.7%, respectively. The total PEM system efficiency is measured at 87.9% at an average input power level of 10 W. The PEM design was able to extract 50% more power than the single-stage converter without energy storage capability. The PEM is also used to demonstrate the flexible resistance control scheme capabilities of the device for broader usage in bioenergy harvesting research.**

***Index Terms*— Battery management systems, biomedical electronics, energy harvesting, intermittent energy storage, mechanical energy.**

I. Introduction

SOCIETY is becoming more dependent on portable personal electronic devices, ranging from medical devices and military equipment to a wide array of consumer electronics. All of these devices are exclusively powered with batteries. Unfortunately, the speed at which new and more powerful electronics are designed is not met with equal speed in the advancement of the battery technology that is used to power these devices. Battery size, weight, and charging time are becoming inconvenient for users. In recent years, there has been increasing interest in the indirect scavenging of energy from everyday human's motions or actions.

The primary hurdle to human energy scavenging is the ability to efficiently produce and store significant power without encumbering the user. Despite being a relatively new field of study, many designs have been produced, which aim to efficiently harvest energy from the average human lifestyle, with power ranging from the microwatt level [1] to the ∼18-W level [2]. Mechanical bioenergy harvesting solutions include shoe mounted designs [3]–[7], such as a linear permanent magnet motor shoe that harvests the energy of the foot during walking producing upward of 0.83 W [7] and knee braces [8], [9] that produce energy from the joint movement of the knee during normal walking, producing upward of 7 or 4.8 W during a generative braking mode. More commonly, many energy harvesters adapt backpack-based energy harvesting systems [2], [10]–[13], utilizing either piezoelectric straps [10], generating 45.6 mW of power with a 45-kg load, or use a spring-based driven damped harmonic oscillator, which can produce up to 18 W of power when excited by a mechanical test bed [2], [11]. Nonmechanical solutions include body-heat thermoelectric generators (21 μW) [14], implantable biofuel cells (20.7 μW) [15], and integrated solar and thermal clothing (500 mW) [16], and generally operate at low power ranges most suitable for wearable sensors. Regardless of the energy source, the majority of these designs use a simple resistive bank to measure the output power of their devices, and all the energies that are generated are lost in the form of heat [4]–[6], [8]–[11], [13]. A few designs do have limited electronic circuitry that is needed to store the harvested energy [2], [7], [12], [17]; however, intermittent power output of the harvester provides a challenge in storing the energy generated. In particular, the peak power generated is often upward of five times of the average power, which drastically increases the necessary size (and weight) of any energy storage capacitors (ESCs).

This paper outlines the design of a two-stage power electronics module (PEM) designed in conjunction with a gear and pulley-based energy harvesting system prototype. Section II describes the design components of the energy harvester system. Section III details the control strategy of the R_{in} controlled boost converter. Section IV examines the buck control strategy. Section V provides an overview of the system design and efficiency. Section VI concludes with a summary of experimentation and objectives.

II. Design and Power Profile of an Energy Harvesting Backpack

A. Mechanical Configuration

The energy harvesting backpack relies on two pulleys that connect to user's ankles by foot harnesses, which extend and

Manuscript received January 23, 2015; revised May 26, 2015 and July 31, 2015; accepted September 29, 2015. Date of publication October 12, 2015; date of current version January 29, 2016. This work was supported by the Natural Sciences and Engineering Research Council of Canada. Recommended for publication by Associate Editor R. C. N. Pilawa-Podgurski.

A. J. Dickson, S. Burton, and Y.-F. Liu are with the Department of Electrical and Computer Engineering, Queen's University, Kingston, ON K7L 3N6 Canada (e-mail: dickson.andrewj@gmail.com; s.burton@queensu.ca; yanfei.liu@queensu.ca).

M. Shepertycky and Q. Li are with the Department of Mechanical Engineering, Queen's University, Kingston, ON K7L 3N6 Canada (e-mail: mshepertycky@gmail.com; q.li@queensu.ca).

Color versions of one or more of the figures in this paper are available online at http://ieeexplore.ieee.org.

Digital Object Identifier 10.1109/JESTPE.2015.2489925

2168-6777 © 2015 IEEE. Personal use is permitted, but republication/redistribution requires IEEE permission.
See http://www.ieee.org/publications_standards/publications/rights/index.html for more information.

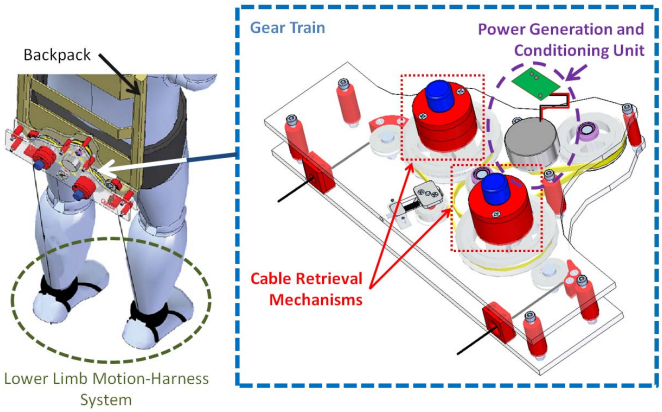

Fig. 1. Mechanical configuration of a 10-W gear-driven energy harvesting backpack.

retract as the user walks. The linear pulley motion is amplified by an internal gear train, which drives a three-phase permanent magnet motor, as shown in Fig. 1.

The energy harvesting backpack targets energy extraction during only the swing phase of a user's walk cycle, as shown in Fig. 2.

The swing phase is targeted in order to produce electrical power while also acting as an assistive device by aiding the user's knee flexor muscles to slow the leg, similar to regenerative braking concepts in electric vehicles. Although the assistive potential of the device is not currently emphasized, the PEM does enable the exploitation of this feature, as outlined in Section III. In this context, generative is characterized by electricity production without requiring additional positive muscle power, as the energy is not repurposed back into the system [8]. Users expend positive energy to accelerate the leg and negative energy to slow limbs. Energy harvester's often target the negative work phase as the available energy stage [18]. This method reduces the impact of the device by introducing minimal resistance during the stance phase, when a user must contract their muscles expending energy to accelerate the leg [8].

The typical voltage waveform from the output of the generator is a variable high-frequency three-phase voltage inside a lower frequency (1–2 Hz) ac envelope similar to the waveform shown in Fig. 3, where the frequency of the outside ac envelope is dependent on the walking speed and step frequency of the user.

The three-phase motor output frequency can vary between 0 and 350 Hz, with 320 Hz being the maximum frequency used experimentally. The peak voltage generated by the energy harvester is 35 V_{l-l} with the peak power around 53 W and with an average power around 14 W at a walking speed of 1.5 m/s (5.4 km/h). Following rectification, the output of the generator may be considered, an approximately 20 V 1–2 Hz rectified sine wave, as shown in Fig. 4, which compares the generator output to a calibrated ac sine wave that mimics ideal operation.

It must be reiterated that the power source for this PEM, the human energy harvester, is very different from the conventional utility grid. With the human energy harvester, the power that is available to be extracted is very limited in comparison with the utility grid, and is time varying at low frequency. All of the powers that are generated come at the expense of a metabolic energy input from the user. It is, therefore, important for the control of this power extraction to be fundamentally different than a conventional battery charger's control scheme. The different sections of the PEM are described in Section III.

B. Biomechanical and Kinematic Considerations

In bioenergy harvesters with human sources, the user's level of effort must be considered. A device's cost of harvest (COH) provides an indication of a harvester's impact on the host, while the kinematics of the device with and without device loading must also be interpreted. The COH is defined as [19]

$$\text{COH} = \frac{P_{\text{met}_{\text{elec}}} - P_{\text{met}_{\text{wwalk}}}}{P_{\text{elec}}} \tag{1}$$

where $P_{\text{met}_{\text{elec}}}$ is the metabolic power of electrical engagement, $P_{\text{met}_{\text{wwalk}}}$ is the metabolic power of weighted walking, and P_{elec} is the system's electrical power, and the metabolic cost of a user is measured using biometric data from breathing patterns during exertion.

The COH provides an indication of a device's mechanical effectiveness, but does not consider the device's metabolic cost of carry (COC) (carrying the weight), as (1) assumes that the device's weight is carried regardless of harvesting. The goal of an energy harvester is to reduce the device's COH, producing maximal electrical energy while impacting the user minimally, such that the extracted energy does not exceed the negative work available [18]. If the targeted harvested energy exceeds the negative work, then the user must expend additional energy to overcome the harvester, which is generally undesirable. The gear-driven energy harvester was tested and averaged over ten young, healthy male subjects (24 ± 3 years old, 1.78 ± 0.08 m tall, and 75.6 ± 10.4 kg) at the Human Performance Laboratory (Hotel Dieu, Kingston), and was tested for normal walking, weighted walking, and mechanical engagement (with the harvester) after an acclimatization period for kinematics, kinetics, and energetics [19]. The harvester's COH results are presented in Fig. 5, and are compared with two energy harvesters operating at similar power levels: 1) the 18-W suspended load backpack [2], [11]; and 2) the 7-W knee brace generator [8], [9].

The mechanical load felt by the user is determined by the emulated resistance of the PEM. A practical experimental range was determined from 19 to 2.5 Ω, where the highest emulated resistance (light load) drew the least amount of current from the generator, thereby requiring less user effort during walking, and the lowest emulated resistance (full load) condition caused the greatest current draw and a higher mechanical resistance. The COH from 19 to 2.5 Ω ranged from -1.8 ± 5.8 to 3.5 ± 2.1, with a mean COH of 0.5 ± 2, when accounting for the metabolic cost of mechanical engagement with respect to the electrical power generated. As such, the lower limb driven harvester uses 0.5 W of metabolic power to generate 1 W of electrical power. This is a lower

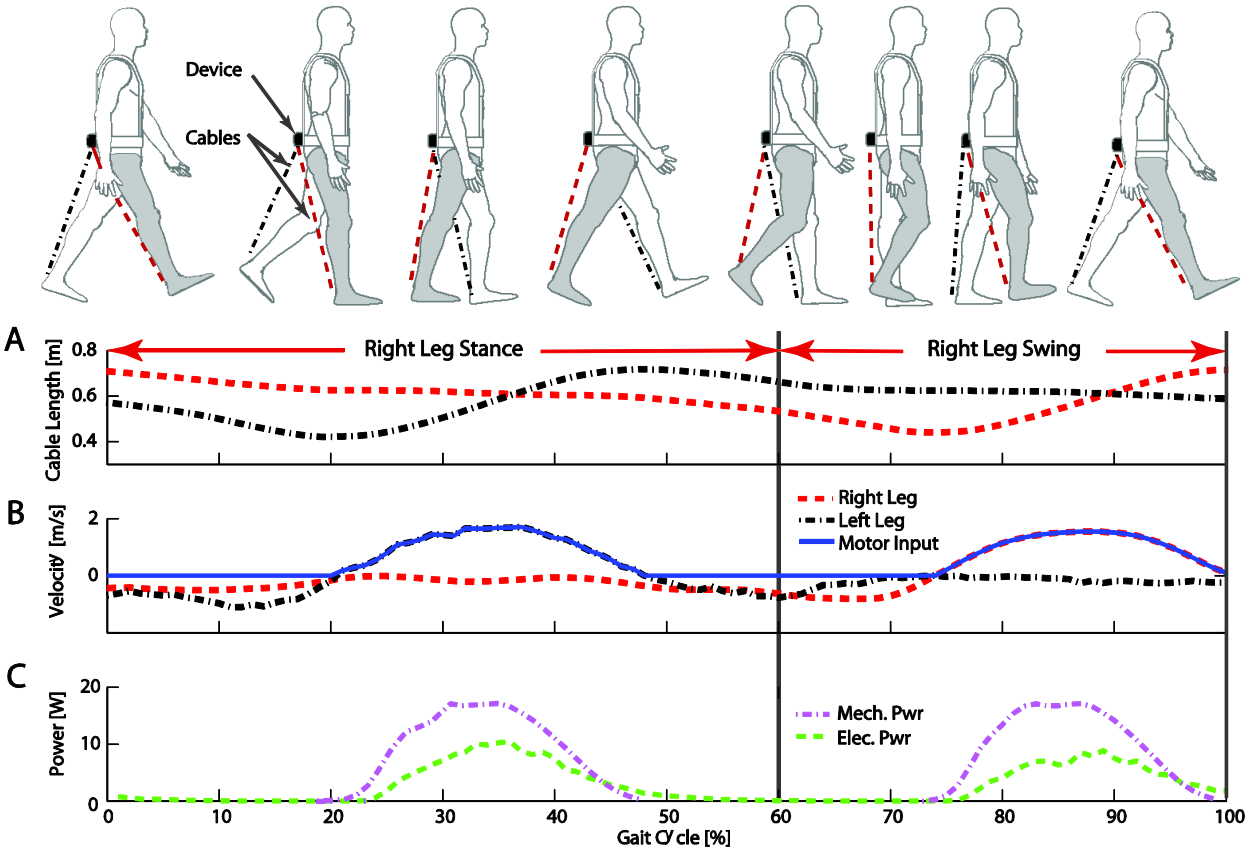

Fig. 2. Voltage profile of a 10-W energy harvesting backpack during stance and swing phases. Red dashed lines: right leg profile. Black dashed and dotted lines: left leg profile in (A) and (B). Purple dashed and dotted: mechanical power, green dashed line: electrical power in (C). (A) shows the cable length for both legs over one gait cycle. (B) shows the cable velocities as well as one summation for one gate cycle. (C) shows the mechanical power inputted into the harvester as well as the electrical power produced. Adopted from [19].

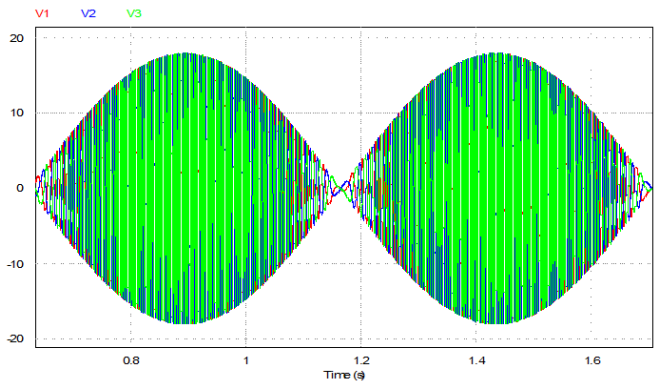

Fig. 3. Typical motor output of the human gait at 1–2-Hz or ∼1.5-m/s walking speed. Ideal simulation without step discontinuity.

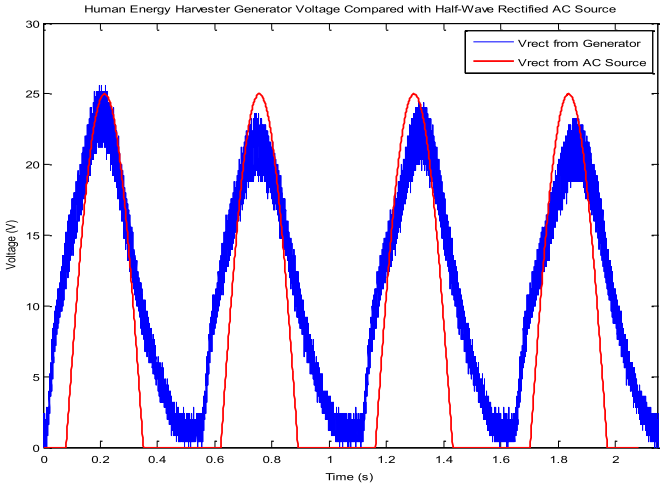

Fig. 4. Rectified three-phase generator output overlaid by a calibrated ac sine wave used for prototyping purposes.

COH than the knee mounted device (0.7) and the suspended backpack (4.8) [19]. These results indicate that the gear-driven energy harvester operates as an assistive device when loaded at 19 and 6 Ω, when the COH is negative. Although the metabolic variance for the 11-Ω loaded case is greater than anticipated, it is within the range for the indirect calorimetry measurements [11], [20] and does not affect the anticipated metabolic trend line, using a quiet standing baseline and the same methodology as previous metabolic studies of interest [21]–[23].

However, it is difficult to measure the assistive nature of a device by the COH alone. The degree to which a device helps to decelerate a limb competes with the device's COC, as well as with the degree to which a device causes muscular cocontraction, wherein user's muscles are working against an imposed force, or even indications that the device works as an assistive device during the positive work phase by reducing cocontractions, as shown in [24] and [25]. In order to further investigate the potential assistive impact of the PEM, a complement of resistive profiles could be generated to the

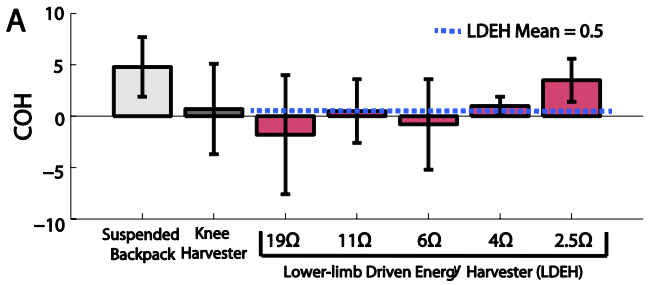

Fig. 5. COH of a 10-W gear-driven energy harvesting backpack (lower limb driven energy harvester) compared with comparable devices at similar power levels (18-W suspended load backpack and 7-W knee brace generator), from 2.5 Ω (full load) to 19 Ω (light load).

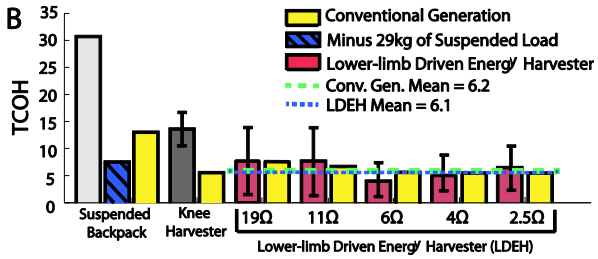

Fig. 6. TCOH of a 10-W gear-driven energy harvesting backpack (lower limb driven energy harvester) compared with comparable devices at similar power levels (18-W suspended backpack and 7-W knee brace generator), from 2.5 Ω (full load) to 19 Ω (light load). Adopted from [19].

user as variable resistances during key phases of the gait cycle using the dynamic R_{in} control mode outlined in Section III-C, while minimally impacting the maximum power extraction scheme. A second metric, the total COH (TCOH) shown in (2), provides a more transparent indication of the device's impact on the user, as it considers the device's COC, which is relative to the speed of carry approximately linearly [26], [27]

$$\text{TCOH} = \frac{P_{\text{met}_{\text{elec}}} - P_{\text{met}_{\text{nwalk}}}}{P_{\text{elec}}} \tag{2}$$

where $P_{\text{met}_{\text{nwalk}}}$ is the metabolic power of normal walking. The TCOH of the gear-driven energy harvester is shown in Fig. 6.

The TCOH for the same range of resistances ranged from 7.7 ± 6.2 to 4 ± 3.6, with a mean of 6.1 ± 1.6, a significant improvement over the knee-mounted device (13.6) and the suspended load backpack (30.7). The complex relationship between an energy harvester and muscular cocontraction is the cause of the discrepancies between the COH and TCOH figures, wherein increasing the resistance felt by the user does not have a linear impact on the user's COH. To this end, current researchers in bioenergy harvesting are interested in learning how the resistance of such devices might be tuned to either harvest the greatest quantities of energy from a user (such as in the scope of this paper), how to generate optimally assistive devices (the intended future research), or a balance of the two. The device's COC was kept low by attaching the mechanics and electronics near to the user's center of mass at the base of a modified backpack, as the metabolic cost of carrying a mass increases distally to a user's center [28]. Note that the conventional generation data (i.e., a hand crank, often used as a comparison in biomechanical harvesters), are defined as [19]

$$\text{COH}_{\text{Conventional Generation}} = \frac{1}{\eta_d * \eta_m} \tag{3}$$

where η_d is the device efficacy at the same electrical resistance and η_m is the peak muscle efficiency when performing positive work (25%) [29]. A comparison with the conventional generation provides an indication of a harvester's viability. Research indicates that when comparing bioenergy harvesters with the equivalent COH of carrying a battery, comparable bioenergy harvesters (6–12 W) may require upward of 260 h of walking to generate the equivalent power provided by a carried battery for an equivalent COH (98 h for a 5.88-kg battery on a 12-W knee harvester, and 227 h for a 6.81-kg battery on a 6-W ankle harvester) [30].

However, bioenergy harvesters have the advantage of being an incidental power source, i.e., the energy is being collected as a consequence of a habitual activity, rather than as a dedicated exercise to generate power. In addition, bioenergy harvesters enjoy the advantage of having a low social stigma (such as the aesthetic debates of solar and wind farms), minimal legislative resistance, and require no additional infrastructure to operate when compared with many other energy harvesting techniques. The long-term viability of such devices is also important to consider, such as in remote locations or during extended hikes.

The device's impact on the kinematics of walking is shown in Fig. 7. The device's impact on joint kinematics (ankle, knee, and hip) is similar to normal walking for the 19 and 11 Ω cases, where the ankle and the knee joint angle begin to deviate at higher resistances. Despite this variance, results indicated that the device contributed between 7% and 24% of the total negative work done by the user's knee during mechanical engagement, as the resistance felt by the user increased. A resistance of 6 Ω was found to be optimal for the conducted trials resulting in the smallest COH (4.0), without significantly impacting the user's gait [19]. The required mechanical input power was lowered by altering subsequent prototypes from a three-stage gear ratio of 18:1 to that of a single-stage 5:1 ratio, which provided a theoretical mechanical efficiency increase of 8.5%, though this did not affect the biomechanical impact of the prototype as the resistances used to load the user were identical [31].

C. Energy Storage Medium

The 16-W spring-oscillating loaded backpack energy harvester [2] provides an example as to why electronic control is so critical to energy harvesting devices at higher powers. In order to capture the peak 50-W power generated by the excited loaded system, researchers required the use of a lithium polymer 152–225-W BB-2590 Bren-Tronics battery pack [32] for a charge rate of 1 C, in addition to filtering from a 5-F 15.2 V ultracapacitor. Due to the intermittent nature of the power source, both components were grossly oversized for the average power of the application, requiring a 3.1-lb battery pack and 12-h charge time during operation to capture the peak energy. This paper provides an elegant alternative to energy

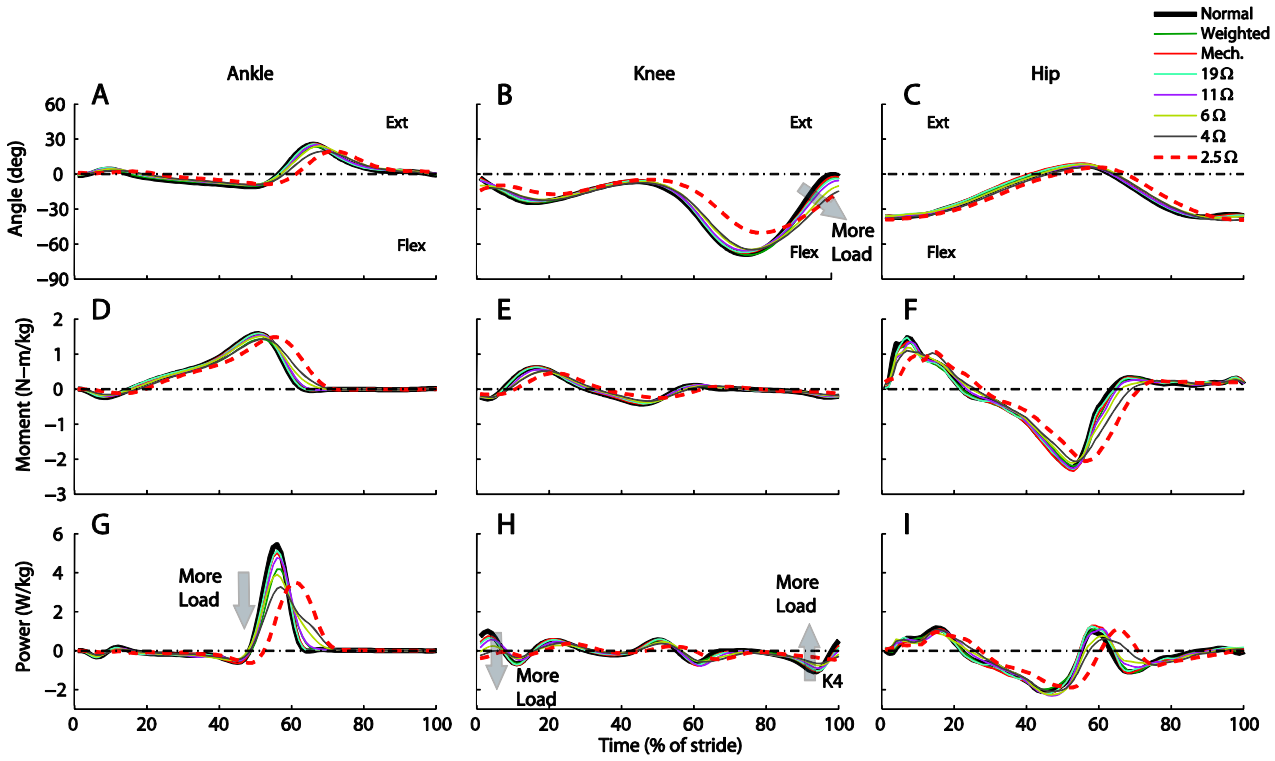

Fig. 7. Kinematics of a gear-driven energy harvester on ten-averaged subjects. A comparison of the joint angle [(A) (B), and (C)], moment [(D) (E), and (F)] and power [(G) (H), and (I)] for the right ankle [(A) (D), and (G)], knee [(B) (E), and (H)] and hip [(C) (F), and (I)] over one gait cycle for eight walking conditions for all resistances (19, 11, 6, 4, and 2.5 Ω trials), plus normal, weighted, and mechanically engaged walking. Adopted from [19].

dumping to remedy the difficulties of peak power extraction in bioenergy harvesting.

The three main categories of rechargeable batteries available are lead-based, nickel-based, and lithium-based batteries, wherein the lithium batteries provide the highest energy density [33]. Ultracapacitors or electrochemical double-layer capacitors (EDLCs) were considered in the design. However, due to the high requirement of voltage of the capacitor and the reduced lifetime of the EDLC, it is not feasible to use these types of capacitors. Instead, we use lithium polymer batteries (LPBs) for the PEM, where the LPB solution allowed for a low system mass/volume ratio when considering the ESC and battery combination, thus minimizing the additional COC. One of the disadvantages of LPB batteries is that they are very sensitive to overcharging. In order to maintain the safety of the battery, the cell voltage must not exceed 4.2 V [34].

P_{battmin}, the minimum value of the maximum battery charging power, can be calculated using (4), where N_{Cells} is the number of cells in the battery pack, $V_{\min}$ is the minimum cell voltage of the battery, R_{batt} is the internal resistance of the battery cell, and I_{CC} is the constant current charging rate of the pack

$$P_{\text{battmin}} = N_{\text{Cells}} * [V_{\min} + R_{\text{batt}} * I_{\text{CC}}] * I_{\text{CC}}. \tag{4}$$

From preliminary experimental trials, the average power generated from the human energy harvester was actually closer to 11.5 W, which can be used to design an appropriate pack capacity for the peak energy storage application. We have chosen to use a battery capacity of 2000 mAh, with a $V_{\min} = 2.8$ V, $R_{\text{batt}} = 0.2$, and $I_{\text{CC}} = 2$ A. To determine the number of cells needed for the worst case, we set $P_{\text{battmin}} > P_{\text{gen-avg}}$ as dictated by

$$N_{\text{Cells}} > \frac{P_{\text{gen-avg}}}{[V_{\min} + R_{\text{batt}} * I_{\text{CC}}] * I_{\text{CC}}}. \tag{5}$$

When calculated, we rounded up to two cells. The nominal voltage of this battery pack is, therefore, 7.4 V, holding 14.8 Wh of energy storage. The range of the maximum charging power of the selected battery pack is from 12.8 to 16.8 W. However, the peak experimental power of the human energy harvester can generate close to 53 W. Without a temporary means of energy storage, the battery pack would need to have five times the capacity in order for it to safely store this peak power that is generated. In a typical walk cycle, the peak power only lasts for a small portion of the power cycle, as shown in Fig. 8. As it is desirable to keep the battery pack small, the PEM must be able to store and release the excess energy.

The PEM stores the extra energy harvested at the boost converter output capacitor or ESC, thus resolving the peak power production.

III. R_{in} Controlled Boost Converter

A boost converter is used as the first stage of the two-stage power converter after the diode rectifier, with the overall PEM layout shown in Fig. 9. The boost converter stage is similar to that of a power factor correction (PFC) boost converter [35] with differences outlined in Table I.

The R_{in} controlled boost converter emulates a resistive load for the generator, with the advantage of the input current

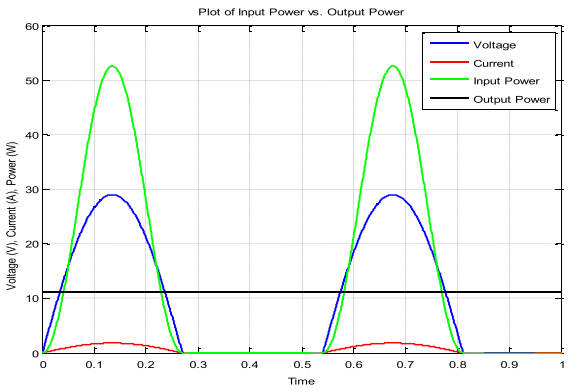

Fig. 8. Simulation of time-varying input energy generated by human energy. Green line (top): input power. Blue line (mid-range): input voltage. Red line (bottom): input current. Black line: average power.

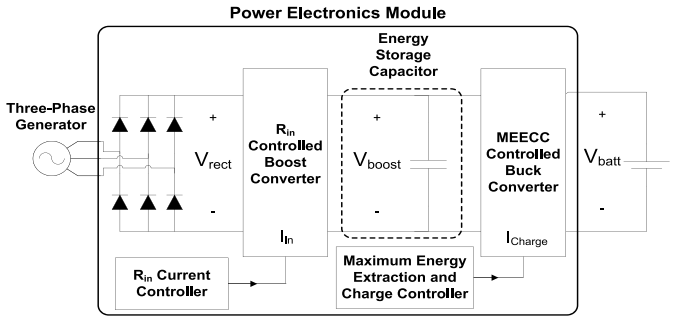

Fig. 9. Two-stage PEM with ESC.

TABLE I

COMPARISON BETWEEN THE CONVENTIONAL PFC AND THE PROPOSED R_{in} CONTROLLED BOOST CONVERTER

	Conventional PFC	Energy Harvesting Boost Converter
Control Parameter	V_{out}	R_{in}
Output Voltage	Regulated	Unregulated
Input Frequency	60Hz	1-2Hz
Seen by Source As	Emulated Resistor defined by V_{out}	Emulated Resistor defined by User

being in phase with the voltage resulting in a high power factor. Unlike typical boost converter topologies, this control method does not regulate the output voltage, but instead utilizes closed-loop feedback to emulate an input resistance desired by the user. The input resistance range was limited to 2.5–19 Ω, based on preliminary human trials, where 2.5 Ω provided an approximate average 10-W average output power, and 19 Ω provided a sufficiently light-load condition where higher resistive values presented a plateau of the power generated. Within this range, the light load should be enforced when the user's instantaneous input voltage is low (during swing phase initiation), and the full-load condition should be applied when the user's instantaneous input voltage is high (during the middle of the swing phase). This variable emulated resistance minimizes the impact of the energy harvester on a user's natural gait cycle during key phases of walking. By controlling the input resistance, the boost converter sees a large output voltage swing that must be minimized by the ESC and regulated by the subsequent buck stage to produce a final stable charging current (CC) for the battery.

As the R_{in} controlled boost converter does not have an outer voltage loop, the boost converter will no longer be responsible for regulating the output voltage V_{boost}. The R_{in} controlled boost converter will only be responsible for extracting current from the generator I_{in} based on the relationship in

$$I_{\text{in}} = \frac{V_{\text{rect}}}{R_{\text{in}}}. \tag{6}$$

However, although the boost output is unregulated, it is still limited by the user-defined input resistance (with a functional range from 2.5 to 19 Ω), as well as implemented current limiting (charging specifications) and overvoltage protection circuitry. The R_{in} controlled boost converter extracts power from the generator according to the user's desired effort level by changing R_{in}. The implemented overvoltage protection for the output of the R_{in} controlled boost converter increases the R_{in} value if the voltage of the ESC reaches its maximum value in order to protect the components. The R_{in} controlled boost converter otherwise satisfies the design requirement of being able to draw current from the generator into any specified profile as determined by the user. The normal operation design requirements of the boost converter are that it must be able to extract the maximum power as defined by the user that is available from the limited power that is generated. The boost converter must also be able to draw current from the generator in any desired wave profile or shape that is defined by the user. In order to meet these design requirement, there are three different control schemes have been developed to control the input current to the boost converter depending on the desired mode of operation: 1) constant R_{in} control; 2) variable threshold R_{in} control; and 3) dynamic R_{in} control.

In particular, the dynamic R_{in} control is of interest in order to lower the user's COH as the resistance felt during a walk cycle is not constant. This feature could be exploited with a dynamic profile to generate an assistive device, rather than a PFC profile which extracts the greatest amount of energy. The initial physical resistance that must be overcome at the beginning of the user's walk cycle should be reduced by simulating a close to open load scenario to minimize the harvester's interference. This will minimize the power extracted from the user, and should be ramped up during the swing phase to achieve a reduced COH. In this way, an adaptive profile can provide a means to generate optimal power levels without unduly burdening the user. In order to meet the design requirements needed to control the input power of the generator and charging rate of the LPBs, the PEM has been designed as a two-stage power converter with an ESC between the two stages and uses a three-phase full-wave Schottky rectifier to rectify the input voltage from the generator.

An active load was considered during the design process; however, it was discounted due to the complexity required to rectify and control the three-phase ac input. The complexity required would improve the efficiency of the diode bridge;

however, it would provide minimal benefit to the final extracted and stored power for two primary reasons. First, the circuit objective is to extract the maximum power from an available, but limited intermittent source. Particularly emphasizing a reduction of the required battery size due to the user's metabolic COC. At low voltages, the available power is very small compared with the power available during peak extraction (which is often dissipated due to the required battery or ESCs). The additional complexity did not warrant adding an active interface for low voltages at this time. Second, during low-voltage periods (particularly at the beginning of the energy extraction when initializing the swing phase), the user is gaining momentum and requires energy to activate their muscles. It is undesirable to impose a resistance during swing phase initialization, but rather to operate under light-load conditions to minimize the impact on the user's gait during windup. The boost converter was designed using the conventional methods [35], [36], and it utilized a 100 V 17-A control nFET and a 100 V 17-A synchronous nFET, with a 40 V 4-A diode for high-side switching and a 180-μH 4-A_{rms} inductor.

A. Constant R_{in} Control

A conventional PFC controller ultimately prioritizes the regulation of the output voltage to reach a constant input resistance at steady state, which is non-optimal for power extraction purposes. Comparatively, the constant R_{in} control scheme enforces a constant input resistance by allowing the output voltage to stabilize instead, which allows the PEM to extract more power from the generator. The constant R_{in} controlled boost converter does not need to regulate its output voltage; therefore, the R_{in} controller can keep the emulated resistance constant. This will allow the constant R_{in} controlled boost converter to extract power from the generator according to the relationship shown in (7), where V_{rect} is the rectified input voltage

$$I_{\text{in}} = \frac{V_{\text{rect}}}{R_{\text{in}}}. \tag{7}$$

The input current waveform will have the same shape as the input voltage. The constant R_{in} controller also has the benefit of the input voltage and current being in phase with each other obtaining a power factor close to unity, thus extracting more real power. The key to extracting the maximum available power from the generator lies in the ability to choose the R_{in} value of the boost converter. The constant R_{in} controller is realized in the digital domain by dividing the sampled input voltage V_{rect} by the desired input resistor value, R_{in}, with the resultant creating the current reference for the boost converter, I_{in}, as shown in Fig. 10.

Ideal experimental verification for this operating mode can be seen in Fig. 11, given $V_{\text{in}} = 30$ V peak, $F_{\text{in}} = 1.85$ Hz, $I_{\text{in}} = 1.5$-A peak, and $R_{\text{in}} = 20\ \Omega$. A half-wave sinusoid emulates an ideal one-legged walk cycle. We can see that the I_{Boost} waveform is the same shape as the input voltage waveform V_{rect}, and based on the waveforms, the converter is emulating a constant resistive load as set by the user.

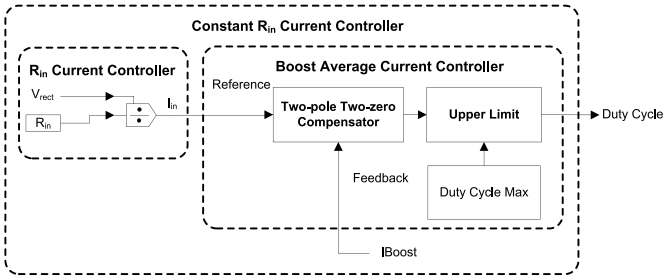

Fig. 10. Constant R_{in} current controller.

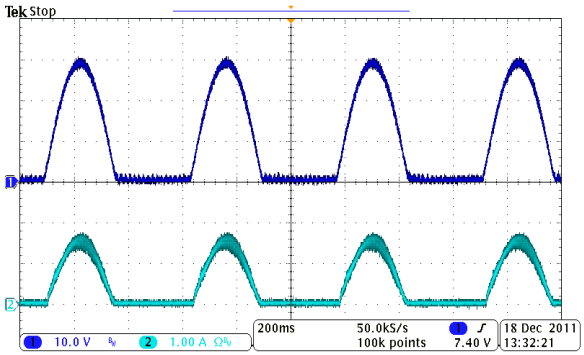

Fig. 11. R_{in} controlled boost converter operating in constant R_{in} control mode. Top: boost converter input voltage. Bottom: boost converter input current. Walk cycle emulated at 1.85 Hz at a switching frequency of 250 kHz.

B. Variable Threshold R_{in} Control

Inside one gait cycle, it is noted that when the input voltage is low, additional mechanical resistance on the user is especially detrimental, and it is, therefore, not desirable to extract a lot of power from user. Comparatively, when the input voltage is high, the user generates a lot of power and more energy can be extracted without impacting user's walking effort. Therefore, to facilitate the user, the next mode of control for the R_{in} controlled boost converter is variable R_{in} control. This mode of control is similar to the constant R_{in} control; however, the value of R_{in} can be changed based on the input voltage level to shape where the majority of the power is extracted during the users gait cycle in order to reduce the walking effort.

The value of R_{in} that is selected can be one of the three values, R1, R2, and R3, depending on the value of the input voltage V_{rect} compared with two threshold voltage levels, V1 and V2, which are preset by the user. Additional resistance thresholds could be selected as desired. The threshold premise block diagram can be seen in Fig. 12.

The variable R_{in} control would be used when it is desired to extract more power from the generator when the input voltage, V_{rect} is higher than the threshold V2 and less power when V_{rect} is between the two threshold values V1 and V2. The variable R_{in} control can also disable the boost converter when the input voltage is too low for conversion, denoted by a V_{rect} less than V1.

An example is configured as follows to demonstrate this control mode, where $V_{\text{in}} = 20$ V peak, $F_{\text{in}} = 1.85$ Hz, $I_{\text{in}} = 2$ A peak, $R_1 = \infty$, $R_2 = 20\ \Omega$, and $R_3 = 10\ \Omega$.

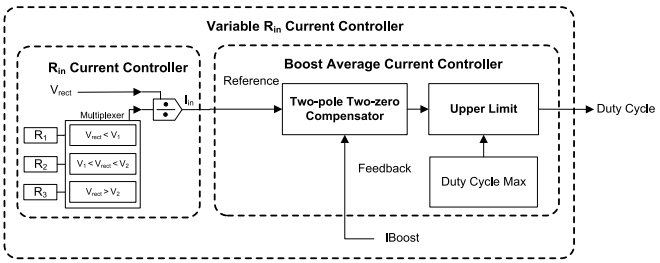

Fig. 12. Variable threshold R_{in} controller.

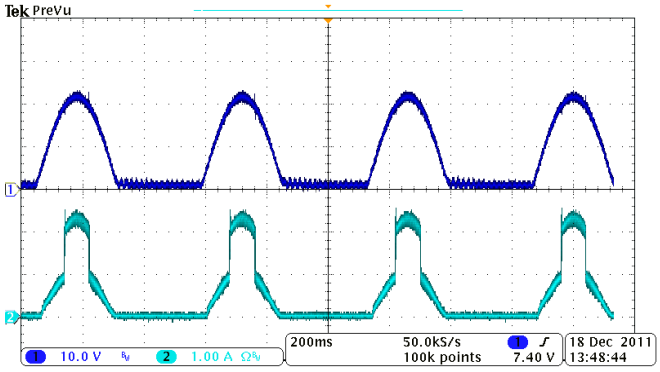

Fig. 13. Variable R_{in} control mode. Top: boost converter input voltage. Bottom: boost converter input current. Walk cycle emulated at 1.85 Hz at a switching frequency of 250 kHz.

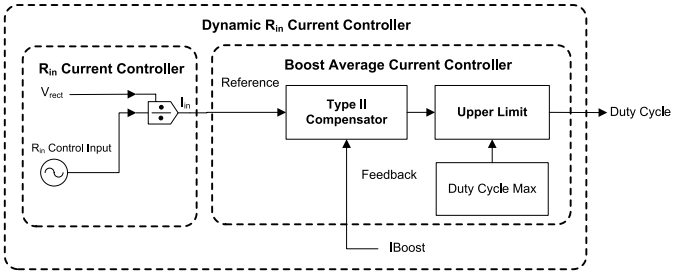

Fig. 14. Dynamic R_{in} controller.

The value of R_{in} is set to be very large when $V_{\text{rect}} < 5$ V, $R_{\text{in}} = 50\ \Omega$ when $5\text{ V} < V_{\text{rect}} < 18$ V and $R_{\text{in}} = 25\ \Omega$ when $V_{\text{rect}} > 18$ V. It can be seen in Fig. 13 that the input power varies with both the input voltage and the input resistor. The current draw is higher when the input voltage is above 18 V and is reduced when the input voltage is between 5 and 18 V. There is no power drawn when the input voltage is below 5 V.

From observing the waveforms of the variable R_{in} control mode, we can see that the controller is emulating three separate resistor values depending on the value of the input voltage.

C. Dynamic R_{in} Control

This mode of control dynamically varies the resistor value of the boost converter directly based on a voltage profile given to the PEM through the use of the analog pin on the analog-to-digital converter (ADC). The input voltage V_{rect} is divided by the sensed R_{in} value, and the result is sent to the Type II compensator as the reference current I_{in} similar to Fig. 12, with a variable waveform in place on the constant R_{in} value, as shown in Fig. 14. This mode of control allows current to be drawn from the generator in any shape or profile, and can

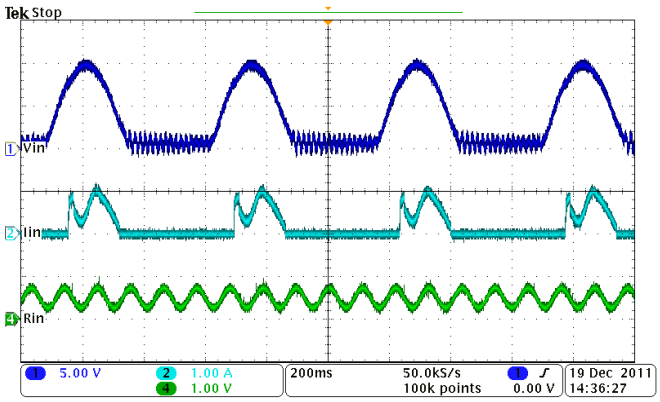

Fig. 15. Dynamic R_{in} control mode. Top: boost converter input voltage. Middle: boost converter input current. Bottom: emulated variable reference resistance. Walk cycle emulated at 1.85 Hz at a switching frequency of 250 kHz.

be tuned to reduce the amount of user energy it requires to drive the generator while still extracting power to optimize the power extracted to energy input ratio or reduce the COH [8].

The profile used for R_{in} is a discontinuous waveform to show that the power draw can be discontinuous, such as during practical experimentation where discontinuity exists in between harvesting periods; the R_{in} value is very large for the first half of the input cycle and is shown as a null waveform. The second half of the cycle is a sinusoid to demonstrate that R_{in} can be any arbitrary waveform. The profile of R_{in} can be of any shape and a sinusoid was shown only for demonstration purposes. Experimental verification is shown in Fig. 15.

We can, therefore, confirm that the dynamic R_{in} controller is emulating the resistor value based on the voltage level on the R_{in} pin of the ADC. R_{in} is sensed identically to the constant and threshold operation methods; however, the variable R_{in} control allows for more flexible resistance control. This method in particular enables kinetics and kinematics research into how resistances introduced at various points during a full walk cycle affect the COH of a bioenergy harvester. The variable resistance profiles introduced are mapped from an analog value to a given load resistance value as required (such as a sinusoid, ramp up, or cutoff profile).

D. Experimental Prototype and Design of the R_{in} Controlled Boost Converter

In order to validate and fine tune the control theories, a prototype with digitally controlled average current mode boost converter was designed with the following design parameters: $V_{\text{in}} = 0 - 35\ V_{\text{rms}}$ with an envelope frequency changing from 0 to 2 Hz. The boost output voltage is not regulated. With the R_{in} control range, the value of V_{boost} will change from 6 to 80 V, given $f_{\text{sw}} = 250$ kHz, $L_{\text{Boost}} = 180\ \mu$H, $C_{\text{Energy Storage Capacitor}} = 2200\ \mu$F, $R_{\text{sense}} = 0.02\ \Omega$, $I_{\text{in}} = 0{-}4$ A, $P_{\text{inpeak}} = 140$ W, and $P_{\text{avg}} = 15$ W. A TMS320F2808 digital signal processor (DSP) was used for the control of the boost converter. The components of the power stage of the boost converter were designed for the converter to operate in continuous conduction mode based on the

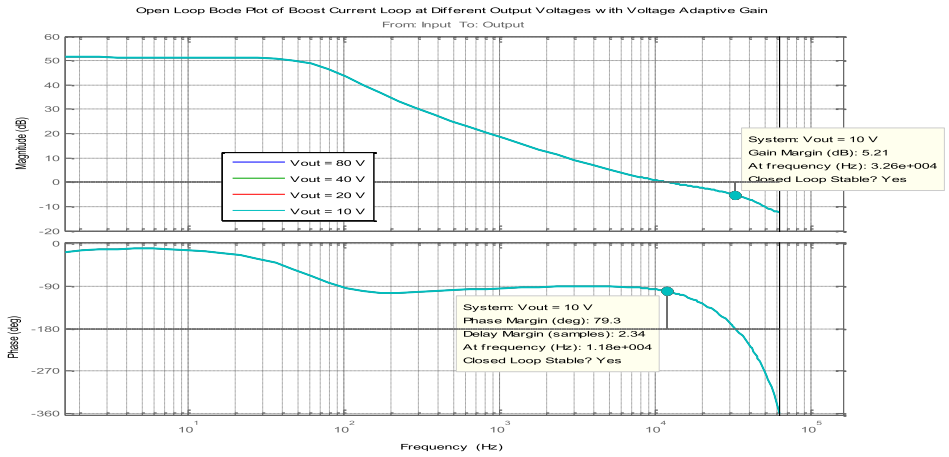

Fig. 16. Open-loop Bode plot of boost controller at different output voltages with a voltage adaptive gain compensator. All four voltage curves follow each other closely.

boost design equations given in [36] (a schematic and printed circuit board was designed with Altium Designer 10 [37], and was populated and debugged in the lab).

The small signal power stage model of the average current mode boost converter, $G_{\text{pboost}}(s)$, was derived in the s-domain from duty cycle to inductor current similar to [38], including parasitic parameters, as shown in (8), shown at the bottom of this page.

After some derivation, the dc gain of the converter can be described by (9), newly defined as the inductor current over the duty cycle

$$\text{dc Gain} = \frac{\widehat{i_L}}{\hat{d}} = 2 \cdot \frac{V_{\text{boost}}}{R_{\text{in}}}. \tag{9}$$

In our energy harvesting application, the boost output voltage changes significantly. In order to achieve wide bandwidth and stability metrics, a controller with a variable gain was designed and used to compensate the system for subsequent stages. This controller with voltage adaptive gain can be expressed in (10), where G_{adp} is the adaptive gain of the compensator, B_2, B_1, B_0, A_2, and A_1 are the controller coefficients, U is the controller output, and E is the error signal

$$\begin{aligned} U(n) = {} & A_1 \cdot U(n-1) + A_2 \cdot U(n-2) \\ & + G_{\text{adp}}(B_0 \cdot E(n) + B_1 \cdot E(n-1) + B_2(n-2)) \end{aligned} \tag{10}$$

where

$$G_{\text{adp}} = 80 \cdot (V_{\text{Boost}})^{-1}. \tag{11}$$

This new controller is applied to the same transfer function $G_{\text{pboost}(s)}$ as before to see the effect of the variable gain controller, as shown in Fig. 16. From Fig. 16, it is observed that the Bode plot for all four output voltage conditions has the same transfer function and performance characteristics, achieving the same performance at high and low output voltage conditions without compromising bandwidth at low output voltages or the phase margin at high output voltages. The variable gain controller can increase the bandwidth at $V_{\text{boost}} = 10$ V from 1.06 to 11.8 kHz with a phase margin of 79.3°. The new variable gain compensator can achieve a turn on time of 5.7 ms under the operating conditions $V_{\text{rect}} = 5$ V and $V_{\text{boost}} = 10$ V.

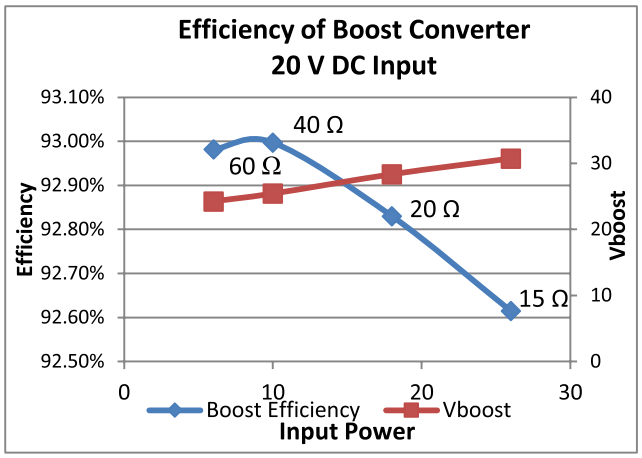

Fig. 17. Boost converter 20 V dc efficiency curve.

E. Boost Converter Efficiency

The dc efficiency of the boost converter was measured operating in constant R_{in} control mode. The efficiency was measured from the input side of the diode rectifier to the output of the boost converter. The emulated input resistor was changed to measure the different efficiencies with the peak efficiency equal to 93% at an emulated resistance of 40 Ω. The boost converter's efficiency curve is shown in Fig. 17.

$$G_{\text{pboost}}(s) = \frac{s \cdot C_{\text{boost}} \left(V_{\text{boost}} \left(1 + \frac{r_{\text{esr}}}{R_L} \right) + I_L \cdot r_{\text{esr}}(1-D) \right) + 2 \cdot I_L(1-D)}{s^2 \cdot L_{\text{boost}} \cdot C_{\text{boost}} \left(1 + \frac{r_{\text{esr}}}{R_L} \right) + s \cdot \left(\frac{L_{\text{boost}}}{R_L} + C_{\text{boost}} \left(R_f \left(1 + \frac{r_{\text{esr}}}{R_L} \right) + r_{\text{esr}}(1-D)^2 \right) \right) + (1-D)^2 + \frac{r_f}{R_L}} \tag{8}$$

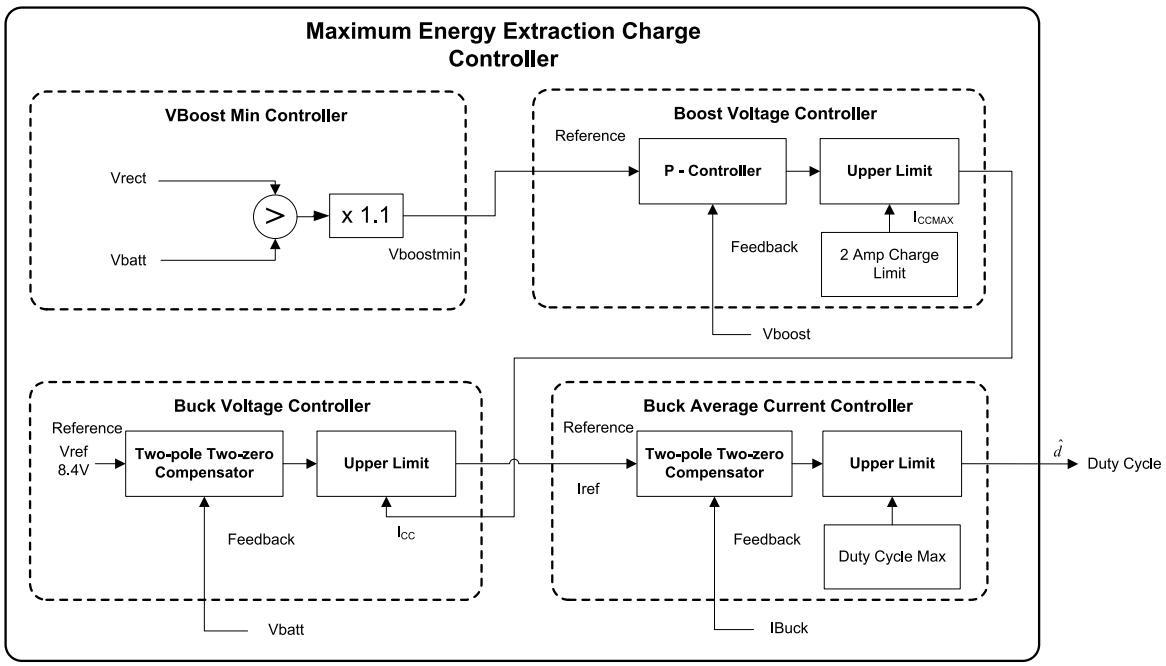

Fig. 18. MEECC block diagram.

IV. Buck Converter Design

The buck converter stage is responsible for minimizing the energy stored in the ESC and regulating the CC of the LPB pack to the CC limit. The buck converter is necessary to step-down the voltage of the ESC to the battery charging voltage, and is responsible for minimizing the energy stored in the ESC by regulating the CC of the LPB pack to the CC limit in order to minimize the voltage stored in the ESC. The minimization of the energy stored in the capacitor is necessary to allow the R_{in} controlled boost converter the more amount of capacity to store the extracted energy from the generator when P_{in} is greater than P_{out}. If the ESC voltage, V_{Boost}, reaches the maximum allowable voltage, V_{Boostmax}, while P_{in} is greater than P_{out}, then we will have to reduce P_{in} so that we do not damage the components. This will cause a reduction in the amount of energy extracted from the generator by the PEM. The energy stored in the ESC is proportional to the voltage of the capacitor squared

$$E = \frac{1}{2}CV^2. \tag{12}$$

The buck converter minimizes this energy by regulating the voltage of the capacitor to its minimum value, V_{Boostmin}. The buck converter also regulates the voltage of the ESC by controlling the CC of the battery as long as the required current to regulate the voltage is within the safe charging limits of the battery. As long as P_{in} is less than P_{out}, the buck will be able to regulate the boost voltage and minimal energy will be stored in the ESC. Once P_{in} becomes higher then P_{out}, the extra energy will need to be temporary stored, and the voltage of the ESC will no longer be regulated by the buck converter and start to increase. The voltage of the ESC will continue to rise as long as P_{in} is greater than P_{out} until it reaches the over voltage protection level, in which case the input power is reduced by the boost converter in order to protect the components. As P_{out} is based on the CC and charging voltage to the battery, P_{out} will vary with the state of charge of the battery. The buck converter was designed using the conventional methods and used a 100 V 17-A control nFET and a 100 V 17-A nFET synchronous nFET, and a 150-μH 5.2-A_{rms} inductor was used.

A. Maximum Energy Extraction and Charge Control Scheme

The most important requirement of the maximum energy extraction and charge controller (MEECC) is the charge regulation of the Li–Po battery pack. The next requirement of the MEECC is to maximize the amount of energy that is extracted and stored into the battery by minimizing the voltage across ESC to its minimum value. These tasks are implemented by four controllers that make up the MEECC and are shown in Fig. 18.

The buck charge controller has two modes of charging: 1) CC mode and 2) continuous voltage (CV) mode. These two modes are controlled using a two loop controller with a current loop and a voltage loop. Note that unlike in maximum energy extraction in solar panels or solar cells, bioenergy harvesters have a nonfixed maximum power point due to their intermittent ac energy source. In this context, the goal of the MEECC is to extract the maximum available power from any given user profile without significantly burdening the user with large ESCs, heavy battery packs, or energy dumping at peak power production. The value of the power extracted is controlled by the user-defined resistance controlled by the first boost stage, whereas the subsequent stages control the charge dissipation and the energy storage.

B. Buck Converter Experimental Verification

In order to validate and fine tune the control theories, a prototype with digitally controlled average current mode

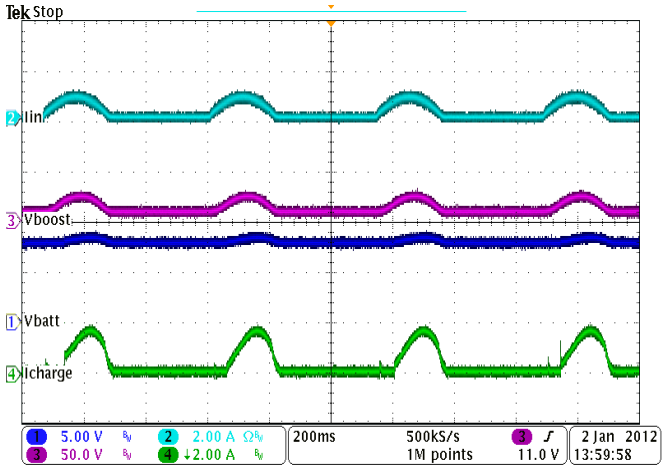

Fig. 19. Buck charging where $P_{\text{in}} < P_{\text{outmax}}$. Top: boost converter input current. Second from top: boost converter input voltage. Second from bottom: battery voltage. Bottom: battery CC.

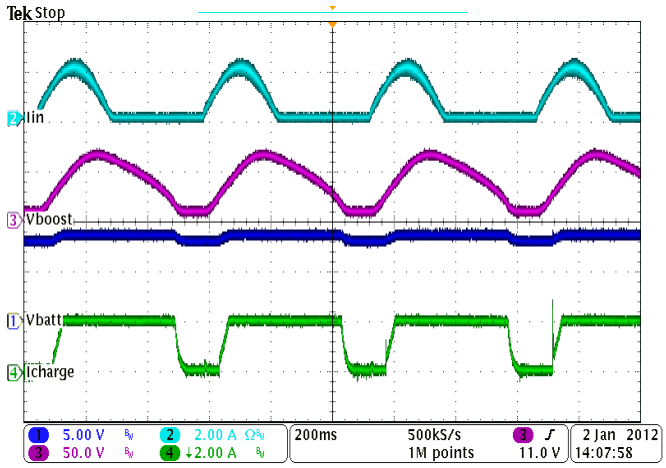

Fig. 20. Battery charging in CC mode with higher P_{in}. Top: boost converter input current. Second from top: boost converter input voltage. Second from bottom: battery voltage. Bottom: battery CC.

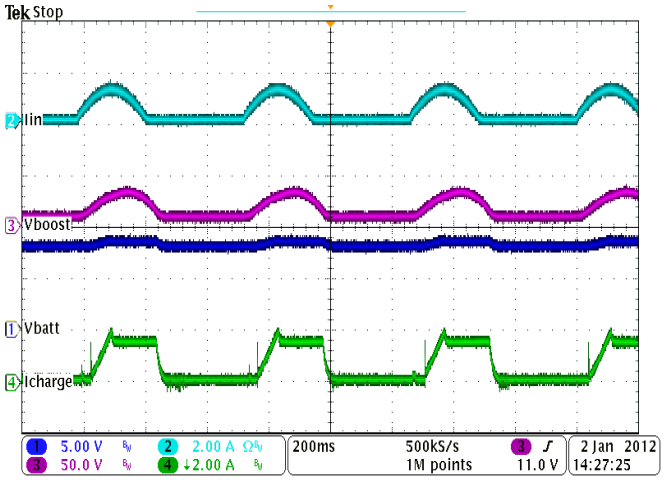

Fig. 21. Battery charging in CV Mode. Top: boost converter input current. Second from top: boost converter input voltage. Second from bottom: battery voltage. Bottom: battery CC.

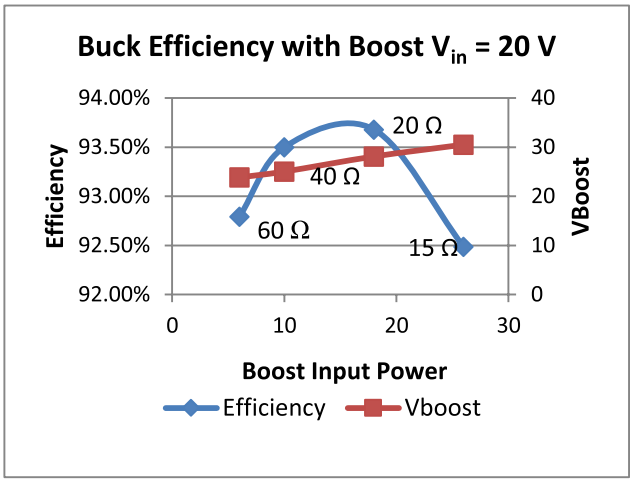

Fig. 22. Buck converter dc efficiency in CC Mode.

buck converter was designed with the following design parameters: $V_{\text{in}} = 6 - 80$ V, $V_{\text{out}} = 5 - 8.4$ V, $f_{\text{sw}} = 250$ kHz, $L_{\text{Buck}} = 150$ μH, $C_{\text{Buck}} = 90$ μF, $R_{\text{sense}} = 0.02$ Ω, $I_{\text{out}} = 0{-}4$ A (limited to 2 A when used with a 2000-mAh battery pack), $P_{\text{outpeak}} = 16.8$ W, and $P_{\text{avg}} = 15$ W. The same TMS320F2808 DSP that was used for the boost converter is also used for the control of the buck converter.

The first waveform capture shown in Fig. 19 demonstrates the buck converter charging the batteries when the generated power is less than the average output power ($P_{\text{in}} < P_{\text{out}}$). The experimental parameters are as follows: $V_{\text{in}} = 17.6$ V peak, $F_{\text{in}} = 1.85$ Hz, $R_{\text{in}} = 24$ Ω, $I_{\text{in}} = 0.8$-A peak, $P_{\text{inmax}} = 14$ W, and $P_{\text{inavg}} = 3.2$ W. From the input current waveform, I_{in}, we can see that the boost converter is operating as expected, when the emulated resistance was set to 24 Ω and the input current is ~0.82-A peak with a maximum input power of 16 W and an average input power of ~3.2 W.

The battery has not reached the maximum CC limit of 2 A during this peak input power. The ESC is not required to store excess peak power when the buck charger has not yet reached its maximum power output.

Fig. 20 was taken when the input power was increased, and the instantaneous input power is greater than the peak output power, with an emulated resistor value of ~16 Ω and a peak battery CC of 2 A. The average input power is 14 W, and the peak power is ~64 W. It is anticipated from this high peak power that the batteries will be charging at their maximum CC rate of 2 A and that the ESC is needed to store the excess peak power.

Fig. 21 shows the battery charging in CV mode.

The boost converter is still emulating a constant resistor value of 18 Ω with a peak input current of 1.16 A while in CV mode. The peak input power is 25 W with the average power around 5.4 W. From the experimental waveforms, it is noted that the MEECC is effective at controlling the buck converter to charge the batteries within their charging limits while extracting the maximum amount of available power. It is noted that the above experimental results are based on charging battery at its maximum allowed rate (two times the discharging current) by adjusting the buck controller. Other battery charging schemes can also be implemented. For example, the battery CC could be maintained at dc level that

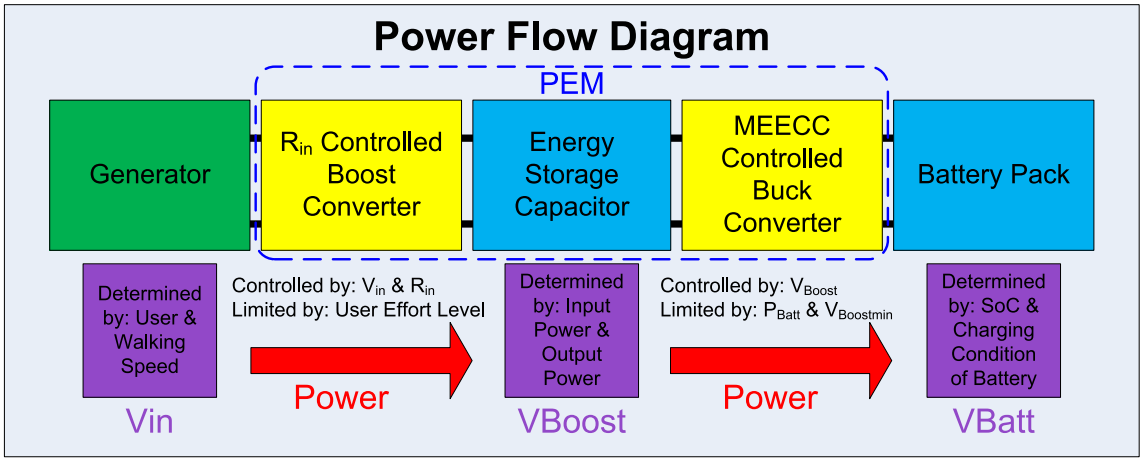

Fig. 23. High-level power flow diagram.

is lower or equal to the maximum CC as necessary.

The dc efficiency of the buck converter was measured with the buck converter operating in constant current charging mode, where the experimental peak efficiency of the buck converter was measured at 93.7% with an emulated input resistance of 20 Ω at an input power of 18 W. The buck converter's efficiency curve is shown in Fig. 22.

V. System Design Notes

As a result of the limited power available for harvest, it is important that the harvested energy be managed efficiently to maximize the usable energy at the output of the PEM. A high-level power flow diagram of the complete system is shown in Fig. 23.

A. Embedded System Software Considerations and ISR Execution Timing

The DSP code was appropriately arranged and optimized in order to reduce the power consumption of the processor in effort to increase the amount of power harvested. To this end, the sampling frequency of the DSP was half that of the switching frequency of the converter, which could still achieve a controller bandwidth of 11 KHz while reducing the power consumption of the ADC and time critical code executions by half. Additional power was saved by disabling all of the peripherals that are not being used by the PEM [39]. These changes reduced the power consumption of the DSP from 1.2 to 0.91 W, a power reduction of 21%.

B. Energy Storage Capacitor Selection

The size of the ESC that was used for the PEM system was 2200 μF. This ESC was capable of storing the excess energy with an input power of 120% of the nominal input power level, while not exceeding 65 V for V_{boostmax} when using the two 2000-mAh battery pack charging in CC mode.

C. Mechanical Rig Testing

A mechanical test rig was used to replicate the power profile generated by a human walking consisting of a three-phase generator coupled to the same dc motor as used in human trials, as shown in Fig. 24.

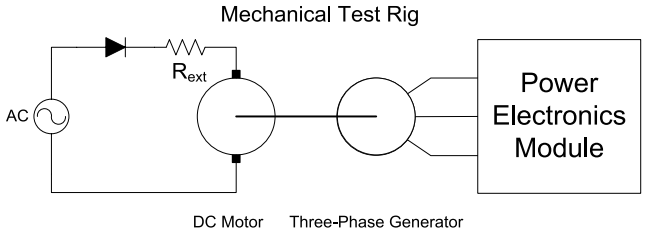

Fig. 24. Mechanical test rig setup.

The mechanical test rig was calibrated to those of the energy harvester's voltage profile as shown in Fig. 4, and was also designed to respond to the effect of the generator being loaded by the PEM and reduce rpm, similar to how a human would feel the resistance of the generator being loaded and the rpm of the generator would decrease. The comparison of the voltage produced by the energy harvester generator with a human walking at a typical walking speed of 1.5 m/s and the voltage produced by the ac source with a diode in series provides a close approximation to the voltage produced by the human energy harvesting generator. The ac source was also designed to remove any inconsistencies in the voltage profile that a human test subject would introduce as well as the ability to conduct experiments without the need of a human test subject to generate the electricity. Fig. 25 shows constant R_{in} control with $V_{\text{in}} = 25$ V. The constant R_{in} controlled boost converter is shown to be drawing current according to a constant emulated R_{in} value for the entire input voltage waveform. When the input power is greater than the output power to the battery the excess energy is stored in the ESC, shown by V_{Boost}. The average output power using the proposed PEM with the ESC is 9 W under these operating conditions.

The R_{in} controlled boost converter was bypassed, and the ESC was removed to test how much power a single-stage buck converter could extract from the same power limited source under the same excitation conditions, given $V_{\text{in}} = 25$ V. The buck charger was used to charge the battery directly from the rectified input voltage to get the waveforms shown in Fig. 26. The buck charger must still abide by the charging regulations of the battery pack and must not exceed the 2-A charge rate.

As can be observed in the I_{in} waveform, the input current is not following an emulated resistance as in the case with the

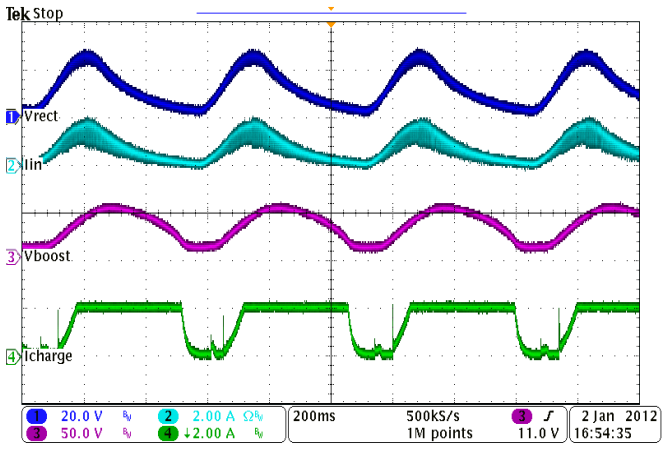

Fig. 25. Constant R_{in} control on a calibrated test rig, designed to mimic the feedback and voltage profile of the energy harvester.

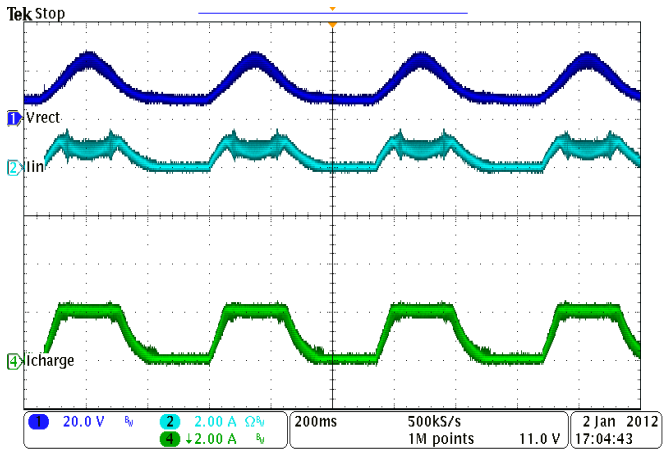

Fig. 26. Constant R_{in} control on a calibrated test rig, designed to mimic the feedback and voltage profile of the energy harvester. Isolated buck energy extraction test case.

R_{in} controlled boost converter enabled, the input current must decrease when the input power is greater than the output power to the battery. The result is less power is extracted from the generator, and therefore, the battery pack is charged at a slower rate. The average output power to the battery is measured at 6.1 W, only 66% of 9 W.

With the R_{in} controlled boost converter, the ESC, and the buck MEECC, the battery pack will charge 150% faster than with a single-stage buck converter. The R_{in} controlled boost converter also provides the advantage of being able to draw current over the entire input voltage waveform increasing the energy extraction as well as allowing the user to control the input current.

An ac test was conducted using the mechanical test rig for the constant R_{in} case where the energy over a full cycle of the input ac waveform was integrated to get the efficiency over that period, and is shown in Fig. 27.

The peak efficiency for $V_{\text{in}} = 15$ V is 91% at $R_{\text{in}} = 60\ \Omega$, $P_{\text{in}} = 0.89$ W, the peak efficiency for $V_{\text{in}} = 20$ V is 90% at $R_{\text{in}} = 60\ \Omega$, $P_{\text{in}} = 1.7$ W, and the peak efficiency for $V_{\text{in}} = 30$ V is 86% at $R_{\text{in}} = 20\ \Omega$, $P_{\text{in}} = 11.5$ W. Efficiency

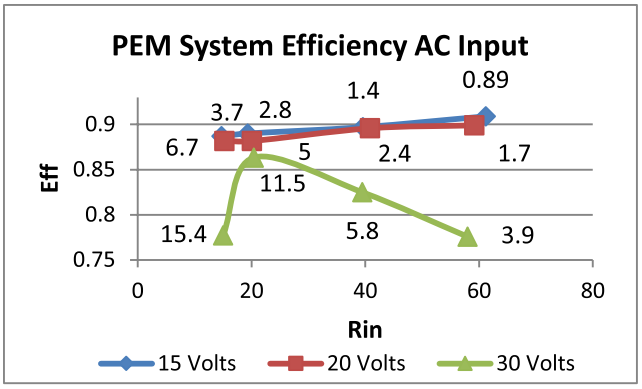

Fig. 27. System efficiency during constant R_{in} testing of a gear-driven energy harvesting backpack.

testing was not conducted for threshold or variable R_{in} cases, as the constant R_{in} case demonstrates the efficiency viability over all operable ranges.

The average output power using the proposed PEM with the ESC was 9 W. The efficiency of the mechanical rig was measured from the input power of the rectifier to the output power of the battery pack with $V_{\text{in}} = 20$ V dc and the boost converter emulating different R_{in} values. The peak efficiency was measured at 87.9% with an emulated input resistance of 40 Ω and an input power of 10 W to the PEM.

VI. Conclusion

A power converter prototype was designed with control algorithms to extract the maximum amount of energy from a human powered energy harvester without overly inhibiting the user. This objective was achieved using a two-stage converter design with energy storage capabilities. The boost converter used three modes of control, all of which are variations on controlling the emulated input resistor value of the boost converter based on the user input value. With this control, the boost converter was able to draw power from the input according to the users desired input level regardless of the output voltage of the boost converter. The buck converter was designed to maximize the power transfer from the output of the first stage and ESC into the battery pack while staying inside the charging limitations of the battery. This objective was accomplished by the design of a maximum energy extraction and charge control algorithm, in which the voltage of the ESC was minimized by transferring all available energy into the battery pack while not exceeding the CC or charging voltage of the battery pack. These objectives were met and verified by experimental waveforms and results. In the future, several improvements could be made to this design. We recommend implementing the following:

1) the P-controller used in the boost voltage controller could be redesigned as a modified PI-controller;
2) different topologies can be explored to replace the boost converter with a bridgeless topology, removing the three-phase diode rectifier;
3) a maximum power point tracking algorithm could sweep the emulated resistor values to maximize the charging power of the battery.

REFERENCES

[1] J. A. Paradiso, "Systems for human-powered mobile computing," in *Proc. 43rd ACM/IEEE Design Autom. Conf.*, Jul. 2006, pp. 645–650.

[2] G. Wang, C. Luo, H. Hofmann, and L. Rome, "Power electronic circuitry for energy harvesting backpack," in *Proc. IEEE Energy Convers. Congr. Expo. (ECCE)*, Sep. 2009, pp. 3544–3549.

[3] J. F. Antaki *et al.*, "A gait-powered autologous battery charging system for artificial organs," *Amer. Soc. Artif. Internal Organs*, vol. 41, no. 3, pp. M588–M595, Jul./Sep. 1995.

[4] S. Ben Ayed, F. Najar, and A. Abdelkefi, "Shape improvement for piezoelectric energy harvesting applications," in *Proc. 3rd Int. Conf. Signals, Circuits, Syst. (SCS)*, Nov. 2009, pp. 1–6.

[5] M. Duffy and D. Carroll, "Electromagnetic generators for power harvesting," in *Proc. IEEE 35th Annu. Power Electron. Specialists Conf. (PESC)*, vol. 3. Jun. 2004, pp. 2075–2081.

[6] J. A. Paradiso and T. Starner, "Energy scavenging for mobile and wireless electronics," *IEEE Pervasive Comput.*, vol. 4, no. 1, pp. 18–27, Jan./Mar. 2005.

[7] Z. Peng, H. Chen, Z. Yang, and A. Khaligh, "Unconventional wearable energy harvesting from human horizontal foot motion," in *Proc. 26th Annu. IEEE Appl. Power Electron. Conf. Expo. (APEC)*, Mar. 2011, pp. 258–264.

[8] J. M. Donelan, Q. Li, V. Naing, J. A. Hoffer, D. J. Weber, and A. D. Kuo, "Biomechanical energy harvesting: Generating electricity during walking with minimal user effort," *Science*, vol. 319, no. 5864, pp. 807–810, Feb. 2008.

[9] Q. Li, V. Naing, J. A. Hoffer, D. J. Weber, A. D. Kuo, and J. M. Donelan, "Biomechanical energy harvesting: Apparatus and method," in *Proc. IEEE Int. Conf. Robot. Autom. (ICRA)*, May 2008, pp. 3672–3677.

[10] J. Granstrom, J. Feenstra, H. A. Sodano, and K. Farinholt, "Energy harvesting from a backpack instrumented with piezoelectric shoulder straps," *Smart Mater. Struct.*, vol. 16, no. 5, pp. 1810–1820, Oct. 2007.

[11] L. C. Rome, L. Flynn, E. M. Goldman, and T. D. Yoo, "Generating electricity while walking with loads," *Science*, vol. 309, no. 5741, pp. 1725–1728, Sep. 2005.

[12] J. Elmes, V. Gaydarzhiev, A. Mensah, K. Rustom, J. Shen, and I. Batarseh, "Maximum energy harvesting control for oscillating energy harvesting systems," in *Proc. IEEE Power Electron. Specialists Conf. (PESC)*, Jun. 2007, pp. 2792–2798.

[13] A. D. Kuo, "BIOPHYSICS: Harvesting energy by improving the economy of human walking," *Science*, vol. 309, no. 5741, pp. 1686–1687, Sep. 2005.

[14] S. E. Jo, M. K. Kim, M. S. Kim, and Y. J. Kim, "Flexible thermoelectric generator for human body heat energy harvesting," *Electron. Lett.*, vol. 48, no. 16, pp. 1013–1015, Aug. 2012.

[15] S. El Ichi *et al.*, "Biocompatible implantable biofuel cell," in *Proc. IEEE Conf. Biomed. Eng. Sci. (IECBES)*, Dec. 2014, pp. 51–55.

[16] Q. Brogan, T. O'Connor, and D. S. Ha, "Solar and thermal energy harvesting with a wearable jacket," in *Proc. IEEE Int. Symp. Circuits Syst. (ISCAS)*, Jun. 2014, pp. 1412–1415.

[17] X. Cao, W.-J. Chiang, Y.-C. King, and Y.-K. Lee, "Electromagnetic energy harvesting circuit with feedforward and feedback dc–dc PWM boost converter for vibration power generator system," *IEEE Trans. Power Electron.*, vol. 22, no. 2, pp. 679–685, Mar. 2007.

[18] Z. Rubinshtein, M. M. Peretz, and R. Riemer, "Biomechanical energy harvesting system with optimal cost-of-harvesting tracking algorithm," in *Proc. 29th Annu. IEEE Appl. Power Electron. Conf. Expo. (APEC)*, Mar. 2014, pp. 3105–3109.

[19] M. Shepertycky and Q. Li, "Generating electricity during walking with a lower limb-driven energy harvester: Targeting a minimum user effort," *PLoS One*, vol. 10, no. 6, p. e0127635, 2015.

[20] Q. Li, V. Naing, and J. M. Donelan, "Development of a biomechanical energy harvester," *J. Neuroeng. Rehabil.*, vol. 6, p. 22, Jun. 2009.

[21] A. D. Kuo, J. M. Donelan, and A. Ruina, "Energetic consequences of walking like an inverted pendulum: Step-to-step transitions," *Exerc. Sport Sci. Rev.*, vol. 33, no. 2, pp. 88–97, 2005.

[22] L. M. Mooney, E. J. Rouse, and H. M. Herr, "Autonomous exoskeleton reduces metabolic cost of human walking during load carriage," *J. Neuroeng. Rehabil.*, vol. 11, p. 80, May 2014.

[23] G. S. Sawicki and D. P. Ferris, "Mechanics and energetics of level walking with powered ankle exoskeletons," *J. Experim. Biol.*, vol. 211, no. 9, pp. 1402–1413, 2008.

[24] H. J. Huang, R. Kram, and A. A. Ahmed, "Reduction of metabolic cost during motor learning of arm reaching dynamics," *J. Neurosci.*, vol. 32, no. 6, pp. 2182–2190, 2012.

[25] M. Darainy and D. J. Ostry, "Muscle cocontraction following dynamics learning," *Experim. Brain Res.*, vol. 190, no. 2, pp. 153–163, 2008.

[26] K. B. Pandolf, B. Givoni, and R. F. Goldman, "Predicting energy expenditure with loads while standing or walking very slowly," U.S. Army Res. Inst. Environ. Med., Natick, MA, USA, Tech. Rep. USARIEM-M-3/77, 1976.

[27] T.-W. P. Huang and A. D. Kuo, "Mechanics and energetics of load carriage during human walking," *J. Experim. Biol.*, vol. 217, no. 4, pp. 605–613, 2014.

[28] R. G. Soule and R. F. Goldman, "Energy cost of loads carried on the head, hands, or feet," *J. Appl. Physiol.*, vol. 27, no. 5, pp. 687–690, 1969.

[29] R. Margaria, "Positive and negative work performances and their efficiencies in human locomotion," *Int. Zeitschrift Angew. Physiol. Einschließlich Arbeitsphysiologie*, vol. 25, no. 4, pp. 339–351, 1968.

[30] E. Schertzer and R. Riemer, "Harvesting biomechanical energy or carrying batteries? An evaluation method based on a comparison of metabolic power," *J. Neuroeng. Rehabil.*, vol. 12, p. 30, Mar. 2015.

[31] M. Shepertycky, "The development and performance evaluation of an energy harvesting backpack," M.S. thesis, Dept. Mech. Eng, Queen's Univ., Kingston, ON, Canada, 2013, p. 84.

[32] Bren-Tronics, Inc. *Datasheet of BB-2590/U*. [Online]. Available: http://www.bren-tronics.com/resource/datasheets/DS-BT-70791CK%20Rev%20B.pdf, accessed: Sep. 10, 2014.

[33] K. L. Stricklett, Ed., *Advanced Components for Electric and Hybrid Electric Vehicles: Workshop Proceedings*, vol. 860. Gaithersburg, MD, USA: National Institute of Standards and Technology, 1994.

[34] S. Dearborn. *Lithium-Ion Battery Charging: Techniques and Trade-Offs*. Microchip Technology, Inc. [Online]. Available: http://techtrain.microchip.com/webseminars/ArchivedDetail.aspx?Active=44, accessed Oct. 1, 2014.

[35] C. P. Basso, *Switch-Mode Power Supplies*. New York, NY, USA: McGraw-Hill, 2008.

[36] B. Hauke, "Basic calculation of a boost converter's power stage," Texas Instrum., Dallas, TX, USA, Appl. Rep. SLVA372C, Nov. 2009.

[37] Altium. *Altium Designer 10*. [Online]. Available: http://products.live.altium.com, accessed Dec. 5, 2014.

[38] L. A. C. Lopes. *Small Signal Model of Boost DC–DC Converter Operating in CCM*, Concordia University. [Online]. Available: http://users.encs.concordia.ca/ lalopes/Courses/ELEC6481-W08/Example233.pdf, accessed Sep. 1, 2014.

[39] Texas Instruments. *Data Manual for TMS320F2808 Digital Signal Processors*. [Online]. Available: http://www.ti.com/lit/gpn/tms320f2808

Andrew Jordan Dickson (S'09) was born in Cobourg, ON, Canada, in 1987. He received the B.Sc. and M.A.Sc. degrees from the Department of Electrical and Computer Engineering, Queen's University, Kinston, ON, Canada, in 2009 and 2012, respectively.

He has been an Advanced Development Electrical Engineer with Alpha Technologies Ltd., Burnaby, BC, Canada, where he is involved in the latest generation of line powering converters, helping to ensure that there is a high degree of reliability and resiliency. In addition, he is also involved in advanced research on the latest generation of hyper efficient rectifiers. His current research interests include digitally controlled battery power management systems for wearable human energy harvesting devices.

Mr. Dickson received the Teacher's Assistant Award in 2011, and the Queen's University Graduate Award in 2009. He was awarded first place in the Queen's University senior year design competition in the Department of Computer and Electrical Engineering.

Sarah Burton received the B.Sc. degree in electrical engineering from Queen's University, Kinston, ON, Canada, in 2013, where she is currently pursuing the M.Sc. degree.

She is a Research Assistant with the Queen's Power Group. Her current research interests include intermittent supply power converters, and electro-mechanical energy harvesting in conjunction with Queen's mechanical engineering.

Ms. Burton received the Teacher's Assistant Award and the McLaughlin Fellowship Award in 2014.

Michael Shepertycky received the B.Sc. and M.Sc. degrees from the Department of Mechanical and Materials Engineering, Queen's University, Kingston, ON, Canada, in 2011 and 2013, respectively, where he is currently pursuing the Ph.D. degree.

He is part of the Collaborative Bio-Medical Engineering program. In collaboration with the Queen's Power Group, he is one of the inventors of the lower-limb driven energy harvester, which is currently patent pending. His current research interests include the energy theories of the human gait.

Mr. Shepertycky received the NSERC Graduate Scholarship in 2015.

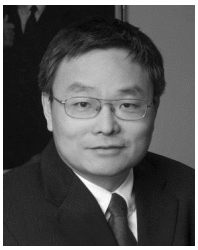

Yan-Fei Liu (M'94–SM'97–F'13) received the Ph.D. degree from the Department of Electrical and Computer Engineering, Queen's University, Kingston, ON, Canada, in 1994.

He was a Technical Advisor with the Advanced Power System Division, Nortel Networks, Mississauga, ON, Canada, from 1994 to 1999. Since 1999, he has been with Queen's University, where he is currently a Professor with the Department of Electrical and Computer Engineering. He has authored over 180 technical papers in the IEEE TRANSACTIONS and conferences, and holds 20 U.S. patents. His current research interests include digital control technologies for high efficiency, fast dynamic response dc–dc switching converter and ac–dc converter with power factor correction, resonant converters and server power supplies, and LED drivers.

Dr. Liu has served as an Editor of the IEEE JOURNAL OF EMERGING AND SELECTED TOPICS OF POWER ELECTRONICS since 2012, and an Associate Editor of the IEEE TRANSACTIONS ON POWER ELECTRONICS since 2001. He served as the Editor-in-Chief of the Special Issue of Power Supply on Chip of the IEEE TRANSACTIONS ON POWER ELECTRONICS from 2011 to 2013. He is also a Principal Contributor for two IEEE standards. He served as the General Co-Chair of ECCE 2015 in Montreal, QC, Canada, and the Technical Program Co-Chair of ECCE 2011. He has served as the Chair of the PELS Technical Committee on Control and Modeling Core Technologies since 2013. He served as the Chair of the PELS Technical Committee on Power Conversion Systems and Components from 2009 to 2012.

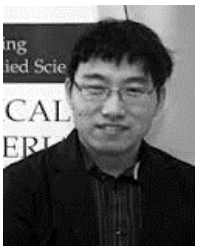

Qingguo Li received the Ph.D. degree from the School of Engineering, Simon Fraser University, Burnaby, BC, Canada, in 2006.

He held a post-doctoral position with the School of Kinesiology, Simon Fraser University, from 2005 to 2008, where he was involved in biome-chanical energy harvesting. He was the Co-Founder of Bionic Power Inc., Vancouver, BC, Canada. He joined Queen's University, Kinston, ON, Canada, in 2009, where he is currently an Associate Professor with the Department of Mechanical and Materials Engineering. His work on energy harvesters has been featured as a peer-reviewed article in the *Journal of Science* and the invention was selected as one of the 50 most important inventions of the year 2008 by the *Time* magazine. He holds three U.S. patents. His current research interests include energy harvesting, wearable robotics, and wearable sensors for human movement analysis.

Dr. Li was a recipient of the Governor General's Gold Medal in 2006.